THE JOURNAL OF PHYSICAL CHEMISTRY B

ARTICLE

pubs.acs.org/JPCB

Sodium Diclofenac and Cell-Penetrating Peptides Embedded in H_{II} Mesophases: Physical Characterization and Delivery

Marganit Cohen-Avrahami, Dima Libster, Abraham Aserin, and Nissim Garti*

The Ratner Chair of Chemistry, Casali Institute of Applied Chemistry, The Institute of Chemistry, The Hebrew University of Jerusalem, Edmond J. Safra Campus, Givat Ram, Jerusalem 91904, Israel

ABSTRACT: Glycerol monooleate (GMO)-based mesophases offer extensive prospects for incorporation of various bioactive molecules. This work deals with the solubilization of selected cell-penetrating peptides (CPPs) together with sodium diclofenac (Na-DFC) within the H_{II} mesophase for transdermal applications. The effect of CPPs such as RALA (an amphipatic CPP), penetratin (PEN), and oligoarginine (NONA) on Na-DFC skin permeation kinetics to provide controlled release and tune the drug transdermal diffusion was studied. The location of the drug and the CPPs within the mesophase was probed by DSC and FTIR. Na-DFC was found to be located at the interfacial region between the surfactant chains, leading to denser H_{II} mesophase. The hydrophilic NONA was intercalated into the aqueous cylinders and caused their swelling. It induced a significant decrease in the hydrogen binding between the GMO carbonyls and their surrounding. The amphiphilic PEN was entrapped within two different regions, depending on its concentration. PEN and NONA improved Na-DFC permeation by 100%, whereas RALA enhanced permeation by 50%. When estimating Na-DFC migration rate out of the mesophase toward surrounding aqueous media, it appeared to be slower with the CPPs. The peptides were not involved at this diffusion-controlled step. It seems that their effect on skin permeation is based on their specific interaction with the skin.

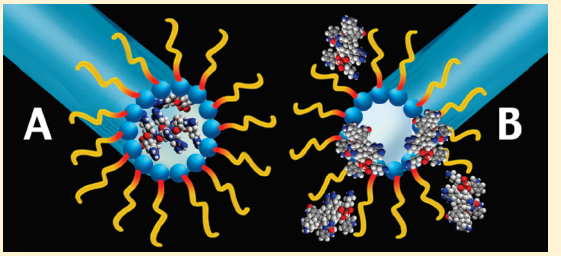

1. INTRODUCTION

Reversed hexagonal (H_{II}) mesophase is interesting and widely studied type of lyotropic liquid crystals with promising potential as drug delivery vehicles.[1] This GMO-based gel-like-structured mesophase offers a variety of advantages, such as ease of preparation, high stability, biodegradability, and mainly a high solubilization capacity for guest molecules within their diverse chemical surroundings.[2] Lyotropic liquid crystals are favorably formed when the amphiphile adopts a wedge shape, with the presence of a solvent, usually water, at specific concentrations.[3,4]

Sodium diclofenac (Na-DFC) is a common NSAID (nonsteroid anti-inflammatory drug) used to treat mild to moderate pain, particularly when inflammation is also present.[5] Its consumed dosage for osteoarthritis or rheumatoid arthritis is 50 mg orally 2−3 times a day or 75 mg orally twice a day. Many classic NSAIDs can cause complications, including ulcers,[6] GI bleeding,[7,8] and some renal function abnormalities.[9] Therefore, improved topical delivery of the NSAIDs would offer an appropriate solution because it would provide the patient with relief without the side effects.[10,11] Some transdermal NSAID formulas that were recently offered[12] were found to be highly efficient in bypassing the complications associated with oral consumption.[13,14] Transdermal drug delivery is an extensively studied area,[15,16] since this is a comfortable and noninvasive route possessing good patient compliance. In particular, the Na-DFC percutaneous penetration can be greatly advantageous because it would preserve its high therapeutic potency and yet avoid hepatic first-pass metabolism and considerable gastrointestinal disturbances.[17] Na-DFC solubility in water is limited to 1113 μg/mL at pH 7.[18] Its chemical structure represents a category of insoluble ion pairs derived from the anion of a weak organic acid and a cation of a strong base. An improvement of its solubility and bioavailability is, therefore, an important task. Different colloidal systems have been used as delivery vehicles for Na-DFC to improve its bioavailability, including microemulsions,[19,20] multiple emulsions,[21] nanoparticles,[22] and others.[23,24] Na-DFC has also been incorporated within lamellar and cubic mesophases, yet its behavior in hexagonal systems has not yet been completely characterized.[25,26]

In this work, Na-DFC was incorporated into the reversed hexagonal mesophase to investigate its transdermal delivery. The exterior skin layer, the stratum corneum, represents the major barrier to the drug permeability through the skin.[27] Three different CPPs[28,29] (cell penetrating peptides) were examined as transdermal delivery enhancers to overcome this barrier, controlling the transdermal penetration rate and tuning it as needed.

The chosen CPPs, representing prominent members of these families, were chosen for their great efficiency and short length; their amino acid sequences are the following:

1 "RALA", RALARALARALRALAR, is a 16-amino-acid peptide belonging to a synthetic family of CPPs, based on GALA, amphipatic peptides named after their alanine-leucine-alanine

Received: December 20, 2010
Revised: June 26, 2011
Published: July 12, 2011

dx.doi.org/10.1021/jp112067v | J. Phys. Chem. B 2011, 115, 10189–10197

repeats that exhibit improved membrane permeability.[30] RALA was developed on the basis of GALA with the addition of the arginine (R) residues that were proved to enhance its cell-penetrative efficiency.[31] The penetration mechanism of these peptides into the cell and into the nucleus was proposed to be based on peptide aggregation within the bilayer surface. When a peptide aggregate reaches a critical size, a transitional destabilization of the membrane bilayers occurs,[32] and a pore is formed. The size of the pore depends on the number of peptides forming it, which limits the size of the molecules that can penetrate through it.[33] RALA was proved to be a highly effective short peptide when incorporated onto liposomal systems,[31] and its advantage as a skin penetration enhancer was recently proved.[34]

2 "PEN", penetratin (RQIKIWFQNRRMKWKK), is a 16-amino-acid sequence based on the active penetrating peptide produced by the homeodomain of the antennapedia homeoprotein.[35,36] Penetratin is named after its ability to penetrate through cell and nuclear membranes[37] and is very popular in the area of drug delivery research and development.[38]

3 "NONA", nona-arginine[39], RRRRRRRRR. Arginine was shown to play a key role in CPP attachment to membranes; thus, much research was done concerning the penetrating activity of polyarginine through membranes.[40] Polyarginine was found to be an effective cell-penetrating peptide.[41,42] The most efficient lengths were 7−9 arginine residues per peptide;[43] thus, the nona-arginine polymer was chosen for this research.

This study utilizes the advantages of the H_{II} mesophase as a transdermal vehicle, in addition to those of the CPPs as skin penetration enhancers, for the development of improved drug delivery vehicles in which the drug diffusion rate might be carefully controlled. The CPPs will be characterized from the aspects of their effect on the drug diffusion kinetics as well as their location within the mesophase and their interactions with its components.

2. MATERIALS AND METHODS

2.1. Materials. Monoolein, GMO, distilled glycerol monooleate (min. 97.1 wt % monoglyceride, 2.5 wt % diglyceride, and 0.4 wt % free glycerol; acid value 1.2, iodine value 68.0, melting point 37.5 °C) was obtained from Riken Vitamin Co. (Tokyo, Japan). Tricaprylin (TAG) (99% purity) was purchased from Sigma Chemical Co. (St. Louis, MO, USA). The water was double-distilled. Sodium diclofenac (Na-DFC) was purchased from Sigma (St. Louis, MO, USA). RALA peptide (>95% purity) was synthesized by American Peptide (Vista, CA, USA). PEN and NONA peptides were purchased from GL Biochem (Shanghai, China). Phosphate buffered saline (PBS) was purchased from Biological Industries (Kibbutz Beit Haemek, Israel). High-performance liquid chromatography (HPLC) grade solvents (water, acetonitrile) were obtained from J.T. Baker (Mallinckrodt Baker, Inc., Phillipsburg, NJ, USA) and Merck (Darmstadt, Germany). Triflouroacetic acid (TFA) was purchased from Fluka (Buchs, Switzerland). All ingredients were used without further purification.

2.2. Methods. *2.2.1. Preparation of H_{II} Mesophases.* The composition chosen for the experiments was based on 73.8 wt % GMO and 8.2 wt % TAG (9:1 weight ratio) at 18 wt % water content. The reverse hexagonal mesophases (H_{II}) were prepared by mixing weighed quantities of GMO and TAG while heating to 45 °C. This was done in sealed tubes under nitrogen atmosphere to avoid oxidation of the GMO. An appropriate quantity of preheated water at the same temperature was added, and the samples were stirred and cooled to 25 °C. Each guest molecule (Na-DFC, RALA, PEN, and NONA) was solubilized to its maximal capacity in each system. The maximal capacity of the systems was determined by measuring the greatest solubilized concentration that did not precipitate or harm the hexagonal structure. The guest molecule was dissolved in water prior to its incorporation into the H_{II} mesophases. As a result of guest molecules' solubilization, the concentrations of GMO and TAG were decreased, keeping their weight ratio and water content constant.

2.2.2. Polarized Light Microscopy (PLM). The samples were inserted between two glass microscope slides and observed with a Nikon Eclipse 80i light microscope (Tokyo, Japan) equipped with cross-polarizers and attached to a Nikon DXM 1200C digital camera and PC-monitor. The samples were analyzed at room temperature.

2.2.3. Small Angle X-ray Scattering (SAXS). Scattering experiments were performed using Ni-filtered CuKα radiation (0.154 nm) from an Elliott rotating anode X-ray generator that operated at a power rating of 1.2 kW. The X-ray radiation was further monochromated and collimated by a single Franks mirror and a series of slits and height limiters and measured by a linear position-sensitive detector. The samples were held in 1.5 mm quartz X-ray capillaries inserted into a copper block sample holder. The temperature was maintained at $T \pm 0.5$ °C with a recirculating water bath. The camera constants were calibrated using anhydrous cholesterol. The scattering patterns were desmeared using the Lake procedure implemented in home-written software.[44] To estimate a lower bound for the sizes of ordered domains (L_H), the full width at half-height of the diffraction peak was measured, and this value was inserted into the Scherrer equation.[45] The error bars were determined according to triplicate measurements of each sample.

2.2.4. Differential Scanning Calorimetry (DSC). A Mettler Toledo DSC822 (Greifensee, Switzerland) calorimeter was used. The DSC measurements were carried out as follows: 25−30 mg H_{II} samples were weighed, using a Mettler M3 microbalance, in standard 40 μL aluminum pans and immediately sealed by a press. The samples were rapidly cooled in liquid nitrogen from 25 to −40 °C at a rate of 10 °C min^{-1}.

The samples remained at this temperature for 30 min and then were heated at 1 °C min^{-1} to 40 °C. An empty pan was used as a reference. The instrument determined the fusion temperatures of the solid components and the total heat transferred in any of the observed thermal processes. The enthalpy change associated with each thermal transition was obtained by integrating the area of the relevant DSC peak. A typical DSC thermogram of an empty H_{II} mesophase consists of two melting events: the first at -1.0 ± 0.3 °C, representing the water fusion; and the second, at $+6.1 \pm 0.3$ °C, representing the melting of probably the eutectic mixture of GMO tails and TAG domains.[46]

2.2.5. Attenuated Total Reflectance Fourier Transform Infrared (ATR-FTIR) Measurements. An Alpha P model spectrometer, equipped with a single reflection diamond ATR sampling module, manufactured by Bruker Optik GmbH (Ettlingen, Germany), was used to record the FTIR spectra. The spectra were recorded with 50 scans at 25 °C; a spectral resolution of

$2\ cm^{-1}$ was obtained. The H_{II} mesophase comprises some major vibration modes, representing the three surfactant chemical environments of the surfactant molecules in the mesophase: the hydrophilic functional groups (the so-called hydrophilic molecular region); the aqueous channels and the GMO hydroxyl headgroups; the interfacial region composed of the carbonyl and ester groups at α, β, and γ positions of the GMO; and the hydrophobic region composed of the GMO tails and TAG.[47]

ATR-FTIR Data Analysis. Multi-Gaussian fitting has been utilized to resolve individual bands in the spectra. The peaks were analyzed in terms of peak frequencies, width at half-height, and area.

2.2.6. In Vitro Skin Penetration Study. Na-DFC permeability through porcine skin was determined in vitro with a Franz diffusion cell system (PermeGear, Inc., Hellertown, PA, USA). The porcine skin was excised from ears of white pigs (locally grown in the Institute of Animal Research, Kibbutz Lahav, Israel), carefully dissected and dermatomized, stored at −20 °C, and used within a month. Before the experiments, the skin was thawed and mounted on Franz cells (diffusion area of 0.635 cm^2) with the stratum corneum facing the donor compartments. The receptor compartment was filled with PBS (pH 7.2). The receptor phase was kept under constant stirring at 37 ± 0.5 °C. A 500 mg portion of the reverse hexagonal mesophases containing 1 wt % Na-DFC and 1 wt % of the various peptides was applied to the surface of the stratum corneum.

Analytical Method. Sodium diclofenac content in the samples was determined by high-performance liquid chromatography (Waters 600 series, Milford, MA, USA) and an autosampler (Waters 717 plus) equipped with a photodiode array detector (Waters 996). Isocratic elution was carried out with 35% acetonitrile and 65% trifluoroacetic acid 0.1% (w/v). The wavelength for UV detection was 275 nm. The column used was a Luna 5 μm, C18, 250 mm ×4.6 mm (Phenomenex, Torrance, CA, USA). The experiments were performed at ambient temperature at a flow rate of 1 mL/min. The injection volume was 50 μL. Retention time of the Na-DFC was 8 min.

Calculation of the In Vitro Data. In the in vitro skin penetration trials using Franz cells, because of the sampling from the receiver solution and replacement with equal volumes of buffer, the receiver solution was constantly being diluted. Considering this, the cumulative drug permeation (Q_t)was calculated from eq 1[48]

$$Q_t = V_r \cdot C_t + \sum_{t=0}^{t-1} V_s \cdot C_i \quad (1)$$

where C_t is the drug concentration of the receiver solution at each sampling time, C_i the drug concentration of the ith sample, and V_r and V_s are the volumes of the receiver solution and the sample, respectively. The obtained data were expressed as the cumulative drug permeation per unit of skin surface area, Q_t/S. The steady-state fluxes (J_{ss}) were calculated by linear regression interpolation of the experimental data (eq 2).

$$J_{ss} = \frac{\Delta Q}{\Delta t \cdot S} \quad (2)$$

Apparent permeability coefficients (K_p) were calculated according to eq 3:

$$K_p = \frac{J_{ss}}{C_d} \quad (3)$$

where C_d is the drug concentration in the donor compartment (1×10^4 μg/mL), while assuming that under sink conditions, the drug content in the receiver was negligible compared with the drug in the donor. The error bars calculation is based on triplicate measurements of each sample.

2.2.7. Na-DFC Release Kinetics Study. "Emptying" experiments of Na-DFC from the H_{II} mesophase to water were performed according to Rizwan et al.[49] as follows: 500 mg of a sample containing 1 wt % Na-DFC without a CPP ("blank") or with each of the CPPs, RALA, PEN, and NONA, were prepared and covered with 10 mL of water and kept at 25 °C. Samples (0.5 mL) of the water were collected at constant times, and the Na-DFC concentration of each sample was determined by a Cary 100 Bio UV−vis spectrophotometer (Varian, Inc., Palo Alto, CA, USA). The Na-DFC concentration was calculated according to the absorption at 275 nm. Each sampling was followed by an insertion of 0.5 mL of fresh water. The same procedure was performed using PBS buffer (pH 7.4) instead of water.

3. RESULTS

3.1. Solubilization Capacities. Each of the guest molecules—Na-DFC, RALA, PEN and NONA—was dissolved in water and solubilized within the H_{II} mesophase. The solubilization capacities as well as the structural effects of the solubilization were determined. It is noteworthy that RALA solubilization and structural characterization were studied previously in our lab;[34] therefore, the structural investigations will focus primarily on PEN and NONA. The effect of RALA will be discussed mostly in the diffusion and skin permeation sections.

The maximum solubilization capacities of each guest molecule within the mesophase was determined by PLM observations and confirmed by SAXS measurements. The maximal solubilization load of Na-DFC, RALA and PEN were found to be 5 wt %. NONA solubilization capacity was 6 wt %.

3.2. Structural Investigation. The structural investigations were carried out by SAXS, DSC, and ATR-FTIR measurements to explore the specific interactions of each guest molecule with the H_{II} components.

3.2.1. The Effect of Na-DFC. When up to 5 wt % Na-DFC was incorporated into the hexagonal mesophase, the hexagonal symmetry was retained. Above this concentration, between 6 and 8 wt % of solubilized Na-DFC, the system lost its hexagonal symmetry, and a dark isotropic phase appeared on the PLM photomicrographs. The SAXS diffractograms of these samples exhibited a single broad peak with d-spacing of 41.3 ± 0.5 Å. This peak seems to belong to a micellar phase formed at these loading concentrations. Above 8 wt %, Na-DFC precipitated from the system.

When analyzing the SAXS data of the Na-DFC-loaded systems at the different concentrations, it was evident that the drug causes shrinkage of the hexagonal channels diameter. The lattice parameter sharply decreases from 57.55 ± 0.5 Å in the blank system to 51.55 ± 0.5 Å in the 5 wt % loaded system (Figure 1), leading to denser packing of the system. Such a "kosmotropic effect" of the Na-DFC might originate from the drug's location between the GMO molecules, causing an enhancement of the interactions between them. This assumption is supported by the slight increase in the domain lengths of the hexagonal clusters in the presence of Na-DFC from 392 to 493 ± 50 Å (Figure 1), hinting a stabilizing effect. The main effect appeared in the low concentration regime, whereas the additional Na-DFC quantities

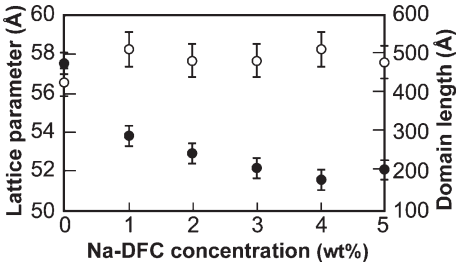

Figure 1. The lattice parameter (●) and the domain length (○) obtained from the SAXS measurements, versus solubilized Na-DFC concentration at the H_{II} mesophases.

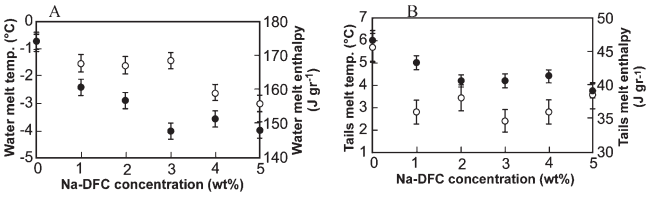

Figure 2. A. The melting point (●) and enthalpy (○) of the aqueous domains versus solubilized Na-DFC concentration in the systems. B. The melting point (●) and enthalpy (○) of the eutectic GMO tails−TAG mixture versus solubilized Na-DFC concentration in the systems.

had a weaker influence. These effects were noticed until the system transformed into a micellar structure.

The DSC measurements reveal a consistent decrease in the water melting point and in its enthalpy in the presence of Na-DFC. The water melting point was decreased from −0.8 to −3.98 ± 0.3 °C, and the melting enthalpy was decreased from 174 to 156 ± 2 J g^{-1} (Figure 2A).

Na-DFC solubilization resulted in an additional effect expressed on the GMO hydrophobic tails. The tails' melting point gradually decreased from 6.1 to 3.8 ± 0.3 °C with the maximum load of Na-DFC, and the melting enthalpy dropped from 45 to 36 ± 2 J g^{-1} (Figure 2B).

These results suggest enhanced water binding in the presence of the drug.[50] Shrinkage of the aqueous columnar cylinders (as detected also by SAXS) caused a change in the structure curvature (curvature more concave toward the inner water phase) and an increase in the fraction of the bound water at the expense of the free water that populated the inner channels. It also indicates that Na-DFC interacts with the surfactant tails, reducing the number of molecules that are free to participate in the melting process.

The analysis of the ATR-FTIR spectra of the H_{II} mesophase with Na-DFC reveals that Na-DFC effect was primarily manifested at the interfacial region. The solubilization caused a remarkable shift in the absorption frequency of the GMO ester O−C═O single bond, from 1184 cm^{-1} in the empty system, with a gradual decrease to a minimal value of 1174 cm^{-1} with 5 wt % Na-DFC (Figure 3).

The low frequency vibration of the CO−O band can be associated with a deviation from the dihedral angle of 180° in this segment, induced by torsional motions, or by a small population of gauche conformers near the α CO−O single bond.[51,52] The low-frequency positions of the CO−O band correspond to more disordered structuring of the lipids. Na-DFC solubilization resulted in a change in the GMO dihedral angle toward a less

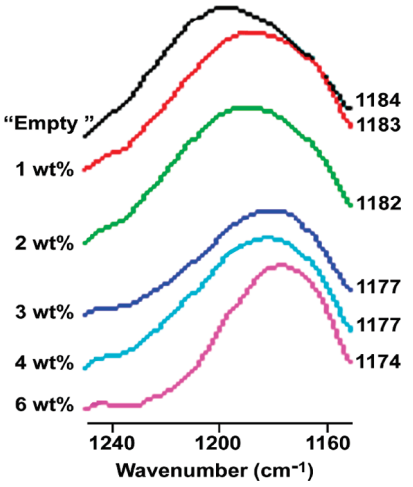

Figure 3. The ATR-FTIR spectra of the "empty system" and Na-DFC-loaded H_{II} mesophases, at the region of the ester bond absorption.

ordered position of CO−O band. There is also an apparent shift in the absorption frequency of the γ C−OH group accompanying Na-DFC incorporation, from 1050 to 1052 cm^{-1}. This shift to higher wavenumbers indicates a decrease in the intermolecular bonds of this functional group. In addition, the tails C−H bending mode at 1460 cm^{-1} revealed a slight and gradual shift to lower wavenumbers, up to 1457 cm^{-1}, implicating an increase in the intermolecular bonds. From these measurements, we can reconfirm the conclusions derived from SAXS and DSC analysis. Na-DFC is intercalated between the GMO molecules. It is located at the interface and influences the intermolecular bonding at this molecular region. It strengthens the interactions between GMO tails, loosens the repulsion tension between the carbon atoms at the headgroups, and enables the formation of a tighter structure with higher curvature. The curvature change increases the freedom between the carbon atoms located at the interfacial region and indirectly induces an increase in the water-binding degree.

3.2.2. The Effect of CPP Load: PEN and NONA. Each CPP was separately solubilized within the H_{II} for identification of its specific location and chemical interactions within the mesophase. The SAXS measurements indicated two trends in the effect of the peptides. Up to 2 wt % of PEN solubilization and initial shrinkage of the aqueous cylinders to a minimum of 53.4 ± 0.5 Å was detected. With increasing solubilization loads of PEN to 5 wt %, the shrinkage changed, and a swelling effect of the cylinders was detected until their diameter reached their original radius of 57.9 ± 0.5 Å (Figure 4).

NONA solubilization had a minor, yet consistent swelling effect on the cylinders. The initial lattice parameter in the blank system was 57.9 ± 0.5 Å, and it slightly increased with NONA loading to a maximal value of 60.5 ± 0.5 Å at 6 wt % NONA.

DSC measurements revealed that both peptides reduced the melting point of the water. The effect of NONA was more pronounced than that of PEN. Whereas the water in the reference system (no CPP) melted at −0.8 ± 0.3 °C, the melting of the system with PEN was reduced to −4.7 ± 0.3 °C. NONA decreased the water melting point to −8.5 ± 0.3 °C (Figure 5A).

Both peptides altered the water melting enthalpy. PEN decreased it from 174 to 102 ± 2 J g^{-1}, whereas in the presence of NONA, it decreased to 66.5 ± 2 J g^{-1} (Figure 5B). The more

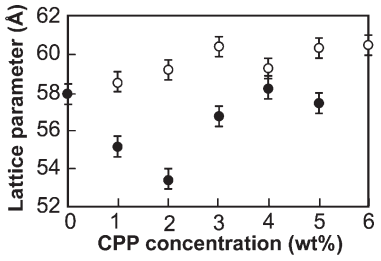

Figure 4. The lattice parameter (α), calculated from the SAXS measurements, versus NONA (○) and PEN (●) concentration in the mesophase.

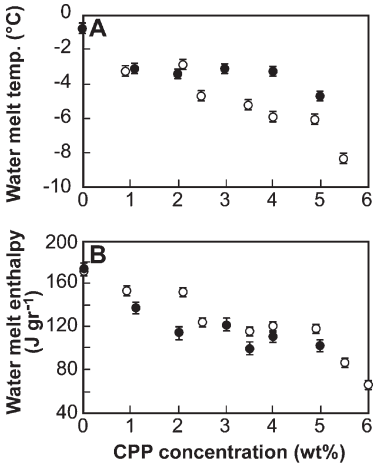

Figure 5. The melting point (A) and enthalpy (B) of the aqueous domains as a function of PEN (●) and NONA (○) concentration in the mesophase.

prominent effect of NONA, which is actually the shorter peptide of the two, on the water binding, is attributed to its high hydrophilicity. The majority of the charged guanidinium groups strongly interact with the water, but PEN, with its amphipatic nature, is coiled in an aqueous medium, limiting its interactions with the water molecules.

The hydrophobic tails of the GMO were only slightly affected by the peptides. Both PEN and NONA slightly decreased the melting point of the oil domains from 6.0 to 4.0 ± 0.3 °C, suggesting some additional spacing between the tails as a result of the CPPs incorporation. The oil melting enthalpy was not affected by the presence of NONA and remained unchanged at 45 ± 2 J g^{-1}, as in the blank system. With PEN, this value decreased to 35 ± 2 J g^{-1} (DSC thermogram not shown). It seems that PEN interacted with the tails, and NONA's effect on this area is very minor.

The ATR-FTIR analysis results showed that PEN strongly affected the interface. Whereas the water O−H groups stretching band did not exhibit any change induced by PEN, the major shifts were on the γ C−OH band, which moved from 1051 to 1054 cm^{-1}, and the C−H bending vibration was at 1381 cm^{-1}, which was gradually shifted to 1423 cm^{-1}. Interestingly, the C−O band shift was most prominent in the initial PEN concentrations, whereas the effect on the γ C−H band was more remarkable at the high PEN loads (Figure 6). This pattern hints an initial solubilization within the more hydrophilic interface, the γ C−OH area, followed by additional solubilization at the C−H

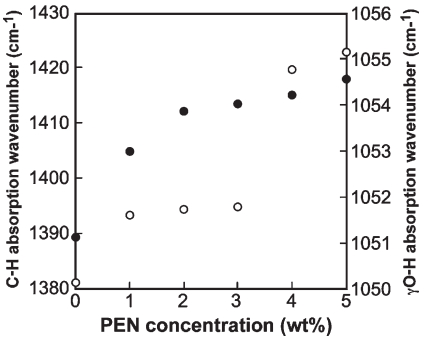

Figure 6. The γ C−OH (●) and the C−H (○) vibration modes as a function of PEN concentration in the mesophase.

area, within the GMO tails. This profile agrees with the SAXS and DSC results showing a two-step PEN solubilization: an initial saturation of the aqueous sites in the channels followed by additional solubilization at the interface.

NONA effect was found to be focused mostly on the water and the GMO carbonyls. The stretching mode of the water was gradually shifted from 3361 to 3346 cm^{-1} with increasing NONA concentration in the mesophase, indicating stronger hydrogen bonding of the water with the peptide. In addition, there is a significant decrease in the ratio between the "bound" carbonyls (absorbing at 1730 cm^{-1}) to the "free" carbonyls (absorbing at 1740 cm^{-1}). In the empty system (no NONA), the ratio between the "bound" and "free" peak areas was 1:8.5, indicating a high degree of hydrogen bonding between the GMO carbonyls and the surrounding water. With NONA, this ratio drops to 1:6, hinting a decrease in the hydration degree of the GMO carbonyls as a consequence of NONA solubilization within the aqueous core. NONA, as shown also by the other techniques, is mostly located in the aqueous core.

Structural investigation revealed that the solubilization sites of the different guest molecules depend on their molecular structure and differ significantly. Na-DFC populates the interfacial region, enhances the interactions between GMO tails, and shrinks and stabilizes the H_{II} mesophase (Figure 7C). PEN solubilization is concentration-dependent. The initial PEN loads populate the hydrophilic headgroup area, whereas the higher PEN loads pack closer to the GMO tails (Figure 7E,F). The hydrophilic NONA populates the inner channels region and swells the mesophase (Figure 7D). It should be noted here that previous investigations on RALA solubilization implied similarly that RALA molecules populate the inner region of the aqueous cylinders, causing their swelling. RALA acts as a chaotropic agent at the H_{II} mesophase, interacting mostly with the water within the channels and enhancing the hydration of the GMO headgroups.[34]

3.2.3. Specific Na-DFC-PEN Interactions. The close interfacial location of PEN and Na-DFC raised the possibility that there might be an interaction between them. We investigated the ATR-FTIR spectra of the combined systems, containing both Na-DFC and PEN, and compared them with those containing only one of these molecules. It is important to note that the complexity of the H_{II} systems limits the number of vibration modes that can be detected for each molecule, revealing only a partial picture of the possible interactions.

The FTIR results did not reveal any significant or specific interactions between Na-DFC and PEN. The typical vibration

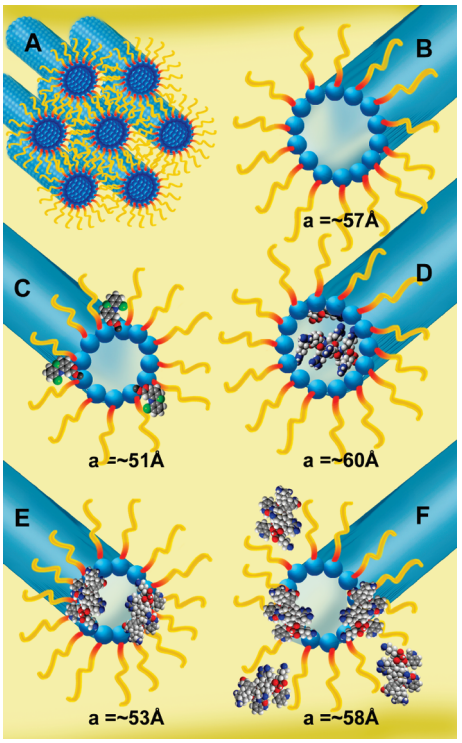

Figure 7. (A) Schematic illustration of the H_{II} mesophase general structure. The water populates the inner region of the cylinders; the GMO tails as well as the TAG point outward. (B) A single "blank", empty system of the H_{II} mesophase, (C) Na-DFC-loaded system. The drug populates the interfacial area and causes channel shrinkage. (D) NONA-loaded H_{II} mesophase. The peptide populates the aqueous channels and swells them. (E, F) PEN-loaded systems. At low PEN concentration (E), it is adsorbed on the GMO headgroups and causes channel shrinkage. With increasing PEN concentration (F), it populates an additional hosting region at the interface.

modes of each molecule remained unchanged with the presence of the other (data not shown). Specific interactions between Na-DFC and PEN will be more deeply investigated in the future, possibly by other techniques.

3.3. The Effect of CPPs on Na-DFC Skin Permeation. The effect of the various peptides on skin permeation efficiency was determined by diffusion experiments of Na-DFC through porcine skin using Franz diffusion cells. All systems were composed of H_{II} mesophases loaded with 1 wt % Na-DFC and 1 wt % of each CPP (the control was a system with Na-DFC and no CPP). We revealed that all three peptides increased significantly the diffusion of Na-DFC through the skin (Figure 8 A).

NONA was found to be the most efficient CPP in enhancing the transdermal penetration because it caused a 2.2-fold increase in the total amount of Na-DFC that diffused through the skin. PEN and RALA caused 1.9- and 1.5-fold increases, respectively, compared with the control system. In all tested systems, there was a gradual and linear increase in the cumulative penetration of Na-DFC with time.

A calculation of Na-DFC percentage that permeated through the skin reveals that at the blank systems, the total amount that diffused through the skin during the 24 h experiment was 0.9% from the initial applied dose. The amount released at the NONA, PEN, and RALA systems was 1.9, 1.8 and 1.3%, respectively. The permeability coefficients (K_p, calculated as $cm \cdot hr^{-1}$), derived

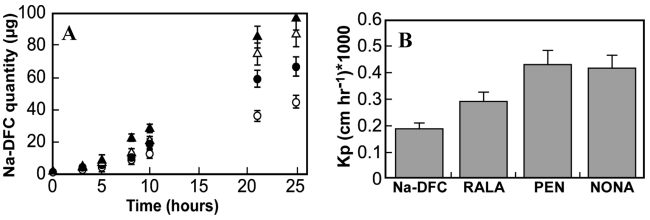

Figure 8. (A) Na-DFC cumulative skin permeation quantity vs time in the different systems: (a) control (Na-DFC only) (○), (b) RALA-loaded (●), (c) PEN-loaded (△), and (d) NONA-loaded (▲). (B) The calculated permeability coefficient (K_p) based on the diffusion rate of 1.0 wt % Na-DFC via Franz diffusion cells as affected by the different peptides added to the mesophase.

from the steady state flux of Na-DFC, revealed the same tendency (Figure 8B), a 1.5-fold increase in the presence of RALA and 2.3- and 2.2-fold increases with PEN and NONA, respectively.

When comparing the efficiency of the more effective CPPs in this experiment, PEN and NONA, we must refer to the different cell-penetration mechanisms of these peptides. Thorén et al. (2005)[53] suggests totally different manners of action for both peptides. Neither peptide creates pores in the cell membranes. Polyarginines (as NONA) enter the cells by direct translocation after causing membrane destabilization. The high positive charge of polyarginine results in a high affinity to the negatively charged membranes. It adheres to the membrane and causes a physical destabilization. The destabilization results in membrane opening and direct translocation of the peptide into the cell. This process is energy-independent.

Penetratin permeation into cells occurs mainly by endocytosis, an energy- and temperature-dependent pathway. The penetratin endocytosis process was suggested also by Drin et al.[54] and by Alves et al.[55] When considering the effect of the peptides on the skin permeability, one can see that despite the chemical differences between them, both peptides have the same "lag time", and their effect is apparent from the fifth hour onward. The chemical nature and loci of the peptides could dictate different diffusion pathways, a diffusion of the polar NONA through the aqueous channels, whereas PEN migration can occur also through the hydrophobic continuous phase. The same lag time of the peptides may hint that the different loci of the peptides within the mesophase did not influence their migration time from the H_{II} toward the skin and that both of them diffused by the same route, causing a similar diffusion rate. The different effect on skin permeability probably results mostly from the interactions with the skin, as supported by their behaviors with cell membranes. Such interactions will be explored in the future.

3.4. Na-DFC Release Kinetics Study. Since the skin permeation studies revealed different profiles for each of the three peptides, we conducted a more detailed analysis using the well established technique of "emptying experiments"[49] (see Section 2.2.7). These experiments aimed to determine whether the rate-determining step of Na-DFC skin permeation from the mesophase is migration out of the mesophase or permeation through the skin. In addition, this analysis provides information on the rate-determining step in the CPP enhancement.

The "emptying" experiments revealed a surprising result. The control system, without CPP, released the largest quantities of Na-DFC with time. The release from the PEN systems was the second in order, whereas NONA and RALA systems released the lowest quantities of Na-DFC (Figure 9 A).

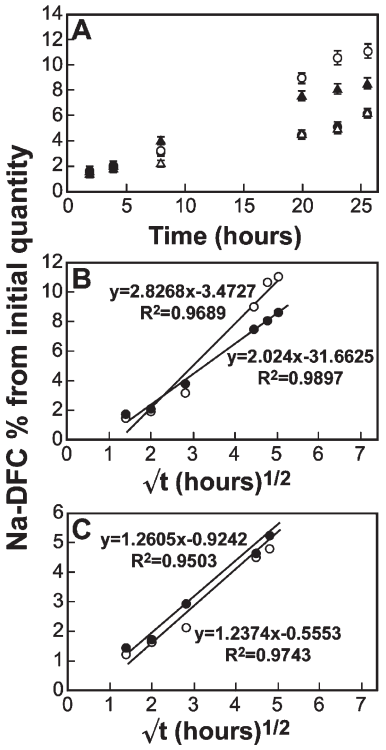

Figure 9. (A) Na-DFC release to water from the H_{II} mesophase containing: (a) no CPP (○), (b) RALA (●), (c) NONA (△), and (d) PEN (▲). Na-DFC release vs the square root of time from (B) the "blank" (no CPP), (○) and PEN (●) systems and (C) RALA (●) and NONA (○) systems.

The diffusion of drugs from different mesophases to water was widely investigated in the past[49] and found to be affected by many factors, including the drug chemical structure, mesophase nanostructure, water content, and surfactant type.[56] Drug release from the various mesophases was found to be primarily controlled by diffusion through the matrix and can be described by the Higuchi[57] diffusion equation:

$$Q = [D_m(2A - C_d)C_d t]^{1/2}$$

Q is the mass of drug released at time t and is proportional to the apparent diffusion coefficient of the drug in the matrix, D_m; the initial amount of drug in the matrix, A; and the solubility of the drug in the matrix, C_d.The slope of a linear fit of the data from this plot is proportional to the "apparent diffusion coefficient" for the drug in the matrix and permits preliminary assessment of diffusion as the primary means of drug release from the correlation coefficient for the linear fit, and second, a means to compare the diffusion of a drug from the different matrices into the release medium. When plotting the weight percentage of released Na-DFC vs the square root of time, a good fit to the Higuchi model was obtained. The linearity of the plots was found to be >0.95 for all CPPs, indicating existence of a diffusion-controlled transport mechanism (Figure 9). The slope was the greatest for the blank system, 2.8 $h^{-1/2}$, and it decreased to 2.0, 1.3, and 1.2 in the PEN, NONA, and RALA systems, respectively.

It is noteworthy that when performing the release experiment with PBS buffer (pH = 7.4) as the release medium, the release profile was very similar. The "blank" systems released the highest amounts of Na-DFC, and the release from the CPP loaded systems was much lower. The order of Higuchi slopes was exactly the same; "blank" > PEN > NONA > RALA, and their values were 3.0, 0.9, 0.7, and 0.6 $h^{-1/2}$, respectively.

4. DISCUSSION

Solubilization of Na-DFC induced a decrease in the lattice parameter derived from closer packing of the cylinders by the interfacially solubilized Na-DFC. The lattice parameter, indicative of the distance between two aqueous channels' centers, decreased because of the enhanced interactions between the tails and the closer packing within the oil continuous phase. Na-DFC amphiphilic molecular structure interacts with the GMO tails, and a small acidic headgroup is locked between the surfactant headgroups. Such interlocked molecules decrease the distance between the aqueous channels. The curvature change was also detected from the DSC measurements, demonstrating an increase in the bound water fraction. The ATR-FTIR vibrational spectra showed greater hydration of the GMO headgroups and a significant shift in the absorption of the O═C−O bond, which is highly indicative of a change in the channels curvature.

Solubilization of Na-DFC into a cubic mesophase was previously investigated in our lab by Efrat et al.[25,26] Na-DFC was found to be a kosmotropic agent at low loading concentrations (up to 0.4 wt %) and a chaotropic agent at greater concentrations (0.4−1.2 wt %). The Na-DFC kosmotropic effect on the cubic phase involved dehydration of the GMO headgroups and shrinkage of the hydrophilic core radius due to a stabilization of the water within the cylinders ("water structure maker"). At concentrations of 0.4 and up to 1.2 wt %, Na-DFC affected mostly the interactions between the micelles, intercalating the micellar aggregates. The cubic symmetry was conserved, but it turned mostly into the so-called bicontinuous cubic structure. High Na-DFC loads (between 1.2 and 12 wt %) resulted in transition to a lamellar phase (strong chaotropic effect). The Na-DFC solubilization effect in our hexagonal systems resembles its effect at the intermediate concentrations on the cubic systems, causing enhanced interactions between GMO molecules toward a denser structure.

Each of the solubilized CPPs is located at a different site within the mesophase. The amphipatic PEN is located close to the headgroup region until saturation and then populates the more hydrophobic region of the interface, intercalated between the carbon atoms of the GMO molecules and toward the tails. The PEN behavior seems to comply with a "site-saturation" behavior. At the low PEN concentrations, PEN populated specific sites within the mesophase, causing greater stability, denser packing, and channel shrinkage. As PEN concentration reached a critical value, the hosting sites were saturated, and the excess PEN molecules were "forced" to populate an "alternative hosting site" within the mesophase. This process was accompanied by cylinder swelling. The hydrophilic NONA is populating the aqueous channels, causing them to swell and loosening the tension between the surfactant molecules. A NONA swelling effect might be attributed to its chaotropic behavior, causing a disorder and destabilization of the "bulk" water within the cylinders. It should be stressed that NONA is a polyarginine, rich in guanidinium moieties, well-known as chaotropic cations.[58,59] The guanidinium ions caused a decrease in the order of the "bulk" water in the channels and displaced it toward the GMO headgroups, resulting in greater hydration of the surfactant and an increase in the channel diameters.

Considering the Na-DFC's amphiphilic nature and the H_{II} mesophase structure, in which the aqueous phase is tightly packed within the lipid structure, with the limited accessibility to the surrounding media, one can assume that the drug diffusion out of the mesophase occurs through the lipophilic oily regions, as suggested by Rizwan et al.[49] The CPPs that are incorporated within the mesophase slow the drug diffusion rate by decreasing its mobility through the mesophase by any specific molecular interfacial interactions. Nevertheless, the emptying experiments showed that the main enhancing effect of the CPPs on skin penetration does not take place in the step of drug migration out of the mesophase. It seems to be due to the enhanced permeation capability of the skin membrane and via any kinetic diffusion controlled process. It should be stressed that RALA and NONA, which populate the inner aqueous channels, revealed a similar diffusion profile with the same slope, $1.2 \pm 0.1\ h^{-1/2}$. PEN that populates the outer interfacial region is less disturbed in its diffusion, causing a release profile with a slope of $2\ h^{-1/2}$. Nevertheless, this interesting mechanism of the drug migration from the H_{II} mesophase in the presence of CPPs molecules cosolubilized within the mesophase should be further investigated.

5. SUMMARY

This work aimed to study the solubilization of Na-DFC and of several cell penetrating peptides in the H_{II} mesophase, and to investigate the skin-penetrating pattern of Na-DFC from the reversed hexagonal mesophase, as affected by the CPPs.

Na-DFC is intercalated between the surfactant chains, mainly in the interfacial region. It enhanced the interactions between GMO molecules toward a denser packing of the nanostructure. Na-DFC solubilization resulted in a noticeable decrease in the lattice parameter and shrinkage of the system toward greater curvature and additional hydration of the GMO headgroups. Specific solubilization capacities of CPP molecules RALA, NONA, and PEN and locations within the mesophase were determined. The results revealed two possible solubilization sites of the peptides within the mesophase: RALA and NONA are located mainly in the aqueous channels, and PEN is first (low loads) solubilized at the headgroup area, interacting with the GMO hydroxyls, until the site reaches saturation, and thereafter (at higher solubilization loads), it is populating the "outer" interfacial region, interacting with the GMO interfacial area.

Skin-penetration efficiency of the CPPs was also evaluated in relation to the type of the CPP molecule. All peptides examined were found to increase Na-DFC permeation through skin. The permeation experiments showed that the permeation was diffusion-controlled, and the CPPs are not involved in the Na-DFC diffusion steps out of the mesophase. The peptides' skin-permeation enhancement is based on the enhanced interaction with the skin. All CPPs delayed drug migration out of the mesophase. The different solubilization sites of the peptides might dictate their different behaviors in the diffusion experiments. The water-soluble peptides had a more pronounced slowing effect on drug diffusion out of the mesophase compared with the minor slowing effect of PEN, which populates the interface. The effect of the CPPs on the skin as well as their specific interactions with the drug and their effect on the drug migration from other mesophases with different characteristics will be further explored in our future studies.

AUTHOR INFORMATION

Corresponding Author

*Phone: +972-2-658-6574/5. Fax: +972-2-652-0262. E-mail: garti@vms.huji.ac.il.

ACKNOWLEDGMENT

The results presented in this manuscript are part of M.C-A.'s dissertation as a partial fulfillment of the requirements toward Ph.D. degree in Applied Chemistry from The Hebrew University of Jerusalem, Israel.

LIST OF ABBREVIATIONS

CPP = cell penetrating peptides
RALA = an amphipatic CPP
PEN = penetratin
NONA = nona-arginine
Na-DFC = sodium diclofenac
GMO = glycerol monooleate

REFERENCES

(1) Achrai, B.; Libster, D.; Aserin, A.; Garti, N. *J. Phys. Chem. B* **2011**, *115*, 825–835.
(2) Ben Ishai, P.; Libster, D.; Aserin, A.; Garti, N.; Feldman, Y. *J. Phys. Chem. B* **2010**, *114*, 12785–12791.
(3) Hato, M.; Yamashita, J.; Shiono, M. *J. Phys. Chem. B* **2009**, *113*, 10196–10209.
(4) Sagnella, S. M.; Conn, C. E.; Krodkiewska, I.; Moghaddam, M.; Drummond, C. J. *J. Phys. Chem. B* **2010**, *114*, 1729–1737.
(5) Mohanambe, L.; Vasudevan, S. *J. Phys. Chem. B* **2005**, *109*, 15651–15658.
(6) Graham, D. Y.; Smith, J. L. *Am. J. Gastroenterol.* **1988**, *83*, 1081–1084.
(7) McCarthy, D. M. *Scand. J. Gastroenterol. Suppl.* **1992**, *192*, 9–16.
(8) Bjaranson, I.; Macpherson, A. J. S. *Pharmacol. Therapeut.* **1994**, *62*, 145–157.
(9) Whelton, A.; Hamilton, C. W. *J. Clin. Pharmacol.* **1991**, *31*, 588–598.
(10) Alexander, K.; Wynn, T. *Int. J. Pharmaceut. Compounding* **2007**, *11*, 181–184.
(11) Fitzpatrick, D.; Corish, J. *Int. J. Pharm.* **2005**, *301*, 226–236.
(12) Banning, M. *Expert Opin. Pharmacol.* **2008**, *9*, 2921–2929.
(13) Baer, P. A.; Thomas, L. M.; Shainhouse, Z. *BMC Musculoskel. Dis.* **2005**, *44*, 44–52.
(14) Guindon, J.; Walczak, J. S.; Beaulieu, P. *Drugs* **2007**, *67*, 2121–2133.
(15) Cheng, Y.; Wu, Q.; Li, Y.; Hu, J.; Xu, T. *J. Phys. Chem. B* **2009**, *113*, 8339–8346.
(16) Gurtovenko, A. A.; Anwar, J. *J. Phys. Chem. B* **2009**, *113*, 1983–1992.
(17) Kigasawa, K.; Kajimoto, K.; Watanabe, M.; Kanamura, K.; Saito, A.; Kogure, K. *Biol. Pharm. Bull.* **2009**, *32*, 684–687.
(18) Llinas, A.; Burley, J. C.; Box, K. J.; Glen, R. C.; Goodman, J. M. *J. Med. Chem.* **2007**, *50*, 979–983.
(19) Lawrence, M. J.; Rees, G. D. *Adv. Drug Delivery Rev.* **2000**, *45*, 89–121.
(20) Kweon, J. H.; Chi, S. C.; Park, E. S. *Arch. Pharm. Res.* **2004**, *27*, 351–356.
(21) Lindenstruth, K.; Muller, B. W. *Eur. J. Pharm. Biopharm.* **2004**, *58*, 621–627.
(22) Beck, R.; Haas, S.; Guterres, S.; Ré, M.; Benvenutti, E.; Pohlmann, A. R. *Quim. Nova* **2006**, *29*, 990–996.
(23) Saravanan, M.; Bhaskar, K.; Maharajan, G.; Pillai, K. S. *Int. J. Pharm.* **2004**, *283*, 71–82.

(24) Cevc, G. *Adv. Drug Delivery Rev.* **2004**, *56*, 675–711.
(25) Efrat, R.; Aserin, A.; Garti, N. *J. Colloid Interface Sci.* **2008**, *321*, 166–176.
(26) Efrat, R.; Shalev, D. E.; Hoffman, R. E.; Aserin, A.; Garti, N. *Langmuir* **2008**, *24*, 7590–7595.
(27) Moore, D. J.; Snyder, R. G.; Rerek, M. E.; Mendelsohn, R. *J. Phys. Chem. B* **2006**, *110*, 2378–2386.
(28) Wang, Q.; Hong, G.; Johnson, G. R.; Pachter, R.; Cheung, M. S. *J. Phys. Chem. B* **2010**, *114*, 13726–13735.
(29) Kaplan, I. M.; Wadia, J. S.; Dowdy, S. F. *J. Controlled Release* **2005**, *102*, 247–253.
(30) Li, W.; Nicol, F.; Szoka, F. C. *Adv. Drug Delivery Rev.* **2004**, *56*, 967–985.
(31) Ambroggio, E. E.; Bagatolli, L. A.; Goormaghtigh, E.; Fominaya, J.; Gasset, M. *Adv. Planar Lipid Bilayers Liposomes* **2007**, *5*, 1–23.
(32) Nir, S.; Nieva, J. L. *Prog. Lipid Res.* **2000**, *39*, 181–206.
(33) Nir, S.; Nicol, F.; Szoka, F. C. *Mol. Membr. Biol.* **1999**, *16*, 95–101.
(34) Cohen-Avrahami, M.; Aserin, A.; Garti, N. *Colloids Surf. B* **2010**, *77*, 131–138.
(35) Letoha, T.; Gaal, S.; Somlai, C.; Czajlik, A.; Perczel, A.; Penke, B. *J. Mol. Recognit.* **2003**, *16*, 272–279.
(36) Polyansky, A. A.; Volynsky, P. E.; Arseniev, A. S.; Efremov, R. G. *J. Phys. Chem. B* **2009**, *113*, 1107–1119.
(37) Deshayes, S.; Morris, M. C.; Divita, G.; Heitz, F. *Cell. Mol. Life Sci.* **2005**, *62*, 1839–1849.
(38) Czajlik, A.; Mesko, E.; Penke, B.; Perczel, A. *J. Peptide Sci.* **2002**, *8*, 151–171.
(39) Sun, J.; Yu, J. S.; Jin, S.; Zha, X.; Wu, Y.; Yu, Z. *J. Phys. Chem. B* **2010**, *114*, 9854–9861.
(40) Tuennemann, G.; Ter-Avetisyan, G.; Martin, R. M.; Stoeckl, M.; Herrmann, A.; Cardoso, M. C. *J. Pept. Sci.* **2008**, *14*, 469–476.
(41) Stewart, K. M.; Horton, K. L.; Kelley, S. O. *Org. Biomol. Chem.* **2008**, *6*, 2242–2255.
(42) Nishihara, M.; Perret, F.; Takeuchi, T.; Futaki, S.; Lazar, A. N.; Coleman, A. W.; Sakai, N.; Matile, S. *Org. Biomol. Chem.* **2005**, *3*, 1659–1669.
(43) Khafagy, E. S.; Morishita, M.; Isowa, K.; Imai, J.; Takayama, K. *J. Controlled Release* **2009**, *133*, 103–108.
(44) Lake, J. A. *Acta Crystallogr.* **1967**, *23*, 191–194.
(45) Amar-Yuli, I.; Wachtel, E.; Ben Shoshan, E.; Danino, D.; Aserin, A.; Garti, N. *Langmuir* **2007**, *23*, 3637–3645.
(46) Amar-Yuli, I.; Wachtel, E.; Shalev, D. E.; Moshe, H.; Aserin, A.; Garti, N. *J. Phys. Chem. B* **2007**, *111*, 13544–13553.
(47) Libster, D.; Ben Ishai, P.; Aserin, A.; Shoham, G.; Garti, N. *Int. J. Pharm.* **2009**, *367*, 115–126.
(48) Sintov, A. C.; Botner, S. *Int. J. Pharm.* **2006**, *311*, 55–62.
(49) Rizwan, S. B.; Hanley, T.; Boyd, B. J.; Rades, T.; Hook, S. *J. Pharm. Sci.* **2009**, *98*, 4191–4204.
(50) Yaghmur, A.; Aserin, A.; Tiunova, I.; Garti, N. *J. Therm. Anal. Calorim.* **2002**, *69*, 163–177.
(51) Hübner, W.; Mantsch, H. H. *Biophys. J.* **1991**, *59*, 1261–1272.
(52) Razumas, V.; Larsson, K.; Miezes, Y.; Nylander, T. *J. Phys. Chem.* **1996**, *100*, 11766–11774.
(53) Thorén, P. E. G.; Persson, D.; Lincoln, P.; Nordén, B. *Biophys. Chem.* **2005**, *114*, 169–179.
(54) Drin, G.; Cottin, S.; Blanc, E.; Rees, A. R.; Temsamani, J. *J. Biol. Chem.* **2003**, *278*, 31192–31201.
(55) Alves, I. D.; Jiao, C. Y.; Aubry, S.; Aussedat, B.; Burlina, F.; Chassaing, G.; Sagan, S. *Biochim. Biophys. Acta* **2010**, *1798*, 2231–2239.
(56) Boyd, B. J.; Whittaker, D. V.; Khoo, S. M.; Davey, G. *Int. J. Pharm.* **2006**, *309*, 218–226.
(57) Higuchi, W. I. *J. Pharm. Sci.* **1967**, *56*, 315–324.
(58) Pegram, L. M.; Record, M. T. *J. Phys. Chem. B* **2007**, *111*, 5411–5417.
(59) Broering, J. M.; Bommarius, A. S. *Biochem. Soc. Trans.* **2007**, *35*, 1602–1605.